IEEE Access
Multidisciplinary | Rapid Review | Open Access Journal

Received 11 September 2022, accepted 29 September 2022, date of publication 6 October 2022, date of current version 14 October 2022.

Digital Object Identifier 10.1109/ACCESS.2022.3212725

RESEARCH ARTICLE

A Fair SINR Performance Comparison of FBMC/OQAM and FBMC/QAM Multicarrier Communication Systems in the Discrete-Time Framework

WAFA KHROUF, (Member, IEEE), MOHAMED SIALA, (Senior Member, IEEE), AND FATMA ABDELKEFI, (Senior Member, IEEE)
MEDIATRON Laboratory, Higher School of Communications of Tunis (SUP'COM), University of Carthage, 2083 Ariana, Tunisia
Corresponding author: Wafa Khrouf (wafa.khrouf@supcom.tn)

ABSTRACT In the last couple of decades, multicarrier modulations have witnessed a considerable interest in wireless communication networks due to their ability to fight against multipath fading and offer multiple access with flexible resource sharing. One of the well known multicarrier modulation systems is filter-bank multi-carrier with an offset quadrature amplitude modulation (FBMC/OQAM), which was proposed as a powerful solution during the standardization of 5G. In this paper, we derive a closed-form expression of the signal to interference plus noise ratio (SINR) for FBMC/OQAM systems in the discrete-time context, for arbitrary wide sense stationary uncorrelated scattering (WSSUS) channels as well as transmitter (Tx) and receiver (Rx) waveforms. We quantify the potential gains in SINR brought by FBMC/OQAM, which exclusively operates on critical lattice density, with respect to FBMC/QAM, which have the flexibility to operate on critical or non-critical lattice densities. For completeness, we compare the performance of FBMC/OQAM in the discrete-time context, sweeping the discrete space of waveforms supports, with that of FBMC/OQAM in the continuous-time context, using the Hermite functions, and show how they perform similarly. Simulation results prove that FBMC/OQAM optimization algorithm, performing with the ping-pong optimized pulse shaping (POPS) paradigm, converges rapidly to excellent SINR values, even with small supports durations, in discrete-time context, which is equivalent to a reduced number of Hermite functions, in the continuous-time context.

INDEX TERMS OFDM, FBMC, OQAM, QAM, interference, SINR, optimization, waveform, POPS algorithm.

I. INTRODUCTION

The need for new applications continues to increase over time and has motivated the researchers to think beyond 5G technology. These applications include extended reality (XR), holographic telepresence, ultra-smart cities, high definition (HD) imaging, remote surgery, distance education, etc [1]. They set different requirements and several criteria [2] that need to be developed while exploring 6G systems, such as:

- Massive asynchronous transmission: For massive machine-type communications (mMTC) services, there will be a high number of nodes communicating over the beyond-5G network. As a consequence, waveforms that have strict synchronization requirements are not suitable for mMTC applications. The most appropriate way to alleviate these synchronization requirements is to use multicarrier systems with well localized waveforms, such as filter bank multi-carrier with offset quadrature amplitude modulation (FBMC/OQAM) waveforms, also known as orthogonal frequency division multiplexing based on OQAM (OFDM/OQAM) [3].
- High spectral efficiency: The spectral efficiency of FBMC systems is proportional to their time-frequency lattice density. Generally, OFDM needs a cyclic

The associate editor coordinating the review of this manuscript and approving it for publication was Zhen Gao.

prefix (CP) insertion, which leads to a reduction in lattice density, hence in spectral efficiency. This can be critical, especially for mobile broadband reliable low latency communication (MBRLLC) because of the resource-limited nature of 6G devices [4]. Therefore, to preserve spectral efficiency, designed systems must operate at critical or close-to-critical lattice densities, without compromising performance. However, the use of CP is essential in this case for OFDM since its waveforms cannot be well localized in time and frequency at the same time, as stated by the Balian-Low theorem [5]. To overcome this problem, we can use FBMC/OQAM, which guarantees a good performance even for moderate to high frequency selectivities, without the need of a CP.

- Extremely low latency: Future applications, such as three-dimensional holographic displays, telesurgery and autonomous driving, target a latency in the order of the sub-ms [6]. Knowing that an optimum decision on a symbol can only be made once the corresponding energy has been totally received, a decision delay of no less than the transmit waveform duration is required. Thus, to reduce latency, one should be able to decrease the duration of waveform support. In other words, it is helpful if we can severely truncate in time the optimized waveforms without leading to perceptible degradation in the SINR. But, the reduction of the support duration of classical OFDM waveform amounts to reducing the useful part of the OFDM symbol and keeping the same CP duration to absorb the channel delay spread, which leads to an increase of the CP overhead. Again, the use of FBMC/OQAM is recommended since the corresponding waveforms are known to be well localized in time and frequency, so they can be severely truncated without degrading the SINR.
- Low device complexity: The Rx complexity depends on the waveforms duration. In fact, the number of multiplications needed for filtering at the receiver is equal to the number of samples of the Rx waveform that is proportional to its duration. Consequently, any reduction in complexity at the Rx must be accompanied by a reduction in the duration of the used waveform. Unfortunately, for classical OFDM, for a critical or close-to-critical lattice, the waveforms are not well localized in time and frequency, which leads in practice to a significant degradation in performance in terms of SINR if a severe truncation is operated. On the other hand, for FBMC/OQAM, the waveforms are so well localized in time and frequency that one can operate with very short durations without being detrimental to the SINR, which makes it possible to have a very reduced reception complexity.

To meet all previous requirements, the FBMC/OQAM remains an interesting candidate for applications beyond-5G, especially within the single-input and single-output (SISO) framework. Consequently, the waveforms optimization is necessary and essential. In this context, several previous works, such as [7], have been led, especially in continuous-time waveforms with infinite supports. The implementation of such functions requires sampling of the optimized waveforms and truncation of their supports. These two operations have the unfortunate trend of breaking the intrinsic properties of optimized waveforms in terms of signal to interference plus noise ratio (SINR) maximization and out-of-band (OOB) emissions reduction. Indeed, sampling causes aliasing, and truncation distorts frequency waveforms, resulting in increased OOB and inter-user interference. In discrete-time context, after optimization, we obtain ready-to-use waveforms, which is not the case of continuous-time systems.

A. RELATED WORK TO FBMC/OQAM OPTIMIZATION

The dominant transmission technique in 4G and 5G networks is OFDM [8] with CP insertion, thanks to its simplicity and to its robustness against multipath fading. Systems or standards, such as asymmetric digital subscriber line (ADSL) and IEEE 802.11a, have already implemented CP-OFDM (also known as OFDM/QAM). However, CP-OFDM causes a loss of spectral and energy efficiencies due to CP insertion, as it contains redundant information. Moreover, the rectangular waveform used in CP-OFDM has a poor frequency localization, making it difficult for designed communication systems to obey stringent specifications on spectrum masks and OOB emissions.

To overcome previously mentioned drawbacks, robust waveform designs have been proposed for beyond-5G networks [2]. In this context, several European projects have been elaborated to design new waveforms for 5G systems, such as FANTASTIC5G [9], METIS [10], and 5GNOW [11]. One of the major proposed candidates was FBMC/OQAM, although it was introduced quite a long time ago (since 1967) [3]. It is now a well established fact that FBMC/OQAM offers the possibility to use time-frequency well-localized waveforms. This allows much better control of OOB emissions and meets stringent spectrum mask requirements. FBMC/OQAM offers also the advantage of suppressing narrow-band interference [12]. In the literature, we find several FBMC/OQAM systems based on different structures and variants. These systems can be classified into two categories: continuous-time and discrete-time systems.

For the continuous-time context, we can cite the isotropic orthogonal transfer algorithm (IOTA) filter [13], which is well localized in time and frequency domains. The underlying IOTA waveform was constructed by performing a double orthogonalization on time and frequency on a Gaussian function. Its good localization and its exponential decay in time and frequency, inherited from the starting Gaussian function, drastically alleviates interference from neighboring symbols in time and frequency [14]. After the discovery of the IOTA waveform, several alternative waveforms, for FBMC/OQAM, offering optimized OOB emissions and bit error rates (BER) [15], or peak to average power ratio (PAPR) [16], have been proposed. In [7], we optimized FBMC/OQAM waveforms in terms of SINR in the continuous-time context.

For the discrete-time context, the PHYDYAS European project [17] waveform, using the Mrabbasi-Martin filter [18], was introduced to reduce OOB emissions. It is also proposed in [19] to reduce the OOB emissions for FBMC/OQAM and universal filtered multi-carrier (UFMC). In [20], the PHYDYAS waveform was optimized in terms of signal to interference ratio (SIR). Other studies in the literature optimized FBMC/OQAM systems in terms of PAPR in [21], as well as OOB and BER in [22].

B. CONTRIBUTIONS

In this paper, we focus on waveforms design and optimization of discrete-time FBMC/OQAM. The orthogonality constraint is limited only to the real field, while for CP-OFDM, it has to be satisfied in the complex field [24].

Our main contributions are the following:

- We provide a new closed-form expression of the SINR, for FBMC/OQAM systems, operating in arbitrary wide sense stationary uncorrelated scattering (WSSUS) [25] channels and Tx and Rx waveforms. We used the ping-pong optimized pulse shaping (POPS) algorithm for the optimization of Tx/Rx waveforms. We recall that the POPS algorithm optimizes the Tx waveform knowing the Rx one, and the Rx waveform knowing the Tx one. Therefore, we need to express the SINR in two different forms: a first form that expresses the SINR as a function of the Rx waveform knowing the Tx one, and another form that expresses the Tx waveform knowing the Rx one. It is emphasized that these two forms of SINR are not symbolically identical, unlike in the continuous case where these two forms are identical.
- We compare, theoretically, the performance of FBMC/OQAM, for critical lattice density, with FBMC/QAM, for critical and non-critical lattice densities, in terms of SINR, in an arbitrary propagation framework, when optimized discrete-time waveforms with finite supports are used.
- In the discrete case, sampled waveforms with finite supports are optimized. Thus, they can be directly used in practice without any subsequent alteration. In contrast, in a previous work in the continuous case [7], waveforms required both sampling and truncation operations for their employability.
- In the continuous case, for the FBMC/QAM, especially for critical and close-to-critical lattice densities, the waveforms are not well localized in time and in frequency, which is in perfect agreement with the Balian-Low theorem [5]. In this case, for FBMC/OQAM, we explored in [7] the space of integrable square functions through the use of a finite number of Hermite functions. Therefore, there is no adequacy with what we want to optimize -which is expected to be not well localized in time and frequency, according to the Balian-Low theorem- and the finite set of Hermite functions that we use to explore the signal space, which are well localized in time and frequency. Since the Hermite functions are well localized in a decreasing order, we do not have to reach a gigantic number of Hermite functions without being able to have a good exploration of the space. Therefore, SINR does not saturate by increasing the number of Hermite functions, as they are not well suited to the space exploration. Thus, we have a precise exploration for FBMC/OQAM and an incomplete exploration for FBMC/QAM. So, the comparison was not fair. In discrete-time, the exploration is precise and fair. In fact, we use the same support duration and the same number of samples for both systems. In addition to that, we have exact values of the SINR in both cases.
- We have noticed in [7] an exponential decrease in time for continuous-time FBMC/OQAM waveforms. We were not able to know if this decay is specific to the optimal waveform, or it is inherited from the exponential decay nature of Hermite waveforms, which were used to explore the signal space for the optimization of these waveforms. In this paper, in discrete-time context, we find again this exponential decay. Therefore, we highlight that this is an intrinsic property of the optimal waveforms. Thus, we have a good localization in time for FBMC/OQAM systems.
- We compare the optimal SINR obtained in continuous-time [7] and discrete-time, for different signal to noise ratio (SNR) values. We note that the exploration of the signals space, in the continuous-time context, showed a superiority of the FBMC/OQAM, compared to the FBMC/QAM, especially in the critical case, since a very reduced number of Hermite functions offers almost the optimal predicted SINR. In this paper, we seek to have an equivalent of this efficiency in the favor of FBMC/OQAM in the discrete-time context. We suspect that this efficiency will be found with very limited supports durations, to reach the optimal SINR, for FBMC/OQAM, compared to FBMC/QAM, which should require very extensive supports durations in time, for a maximum asymptotic SINR.

C. ORGANIZATION OF THE PAPER AND NOTATIONS

This paper is organized as follows. In Section II, we present the adopted system model for FBMC/OQAM and FBMC/QAM in discrete-time context. Then, in Section III, we focus on the derivation of the useful, interference, and noise powers. We derive, in Section IV, the two slightly different forms of SINR expression that allow to optimize the waveforms of Tx knowing those of Rx and vice versa for FBMC/OQAM systems. In Section V, we describe the discrete-version of the POPS algorithm to design optimal waveforms. We dedicate Section VI to the illustration of the obtained analytical results. Finally, we present our conclusion in Section VII.

1) NOTATIONS

Boldface lower and upper case letters refer to vectors and matrices, respectively. The superscripts $.^*$, $.^T$ and $.^H$ refer

to the element-wise conjugation, the transpose and the conjugated transpose of a vector or matrix, respectively. We denote by $v = (\ldots, v_{\eta(-1)}, v_{\eta(0)}, v_{\eta(1)}, \ldots)^T = (v_{\eta(q)})_{q\in\mathbb{Z}} = (v_{\eta(q)})_q$ an infinite vector with q^{th} component $v_{\eta(q)} = [v]_{\eta(q)} = v[\eta(q)]$, and by $M = (M_{\eta(p)\chi(q)})_{p\in\mathbb{Z},q\in\mathbb{Z}} = (M_{\eta(p)\chi(q)})_{pq}$ an infinite matrix with $(p,q)^{\text{th}}$ entry $M_{\eta(p)\chi(q)} = [M]_{\eta(p)\chi(q)}$, where η and χ are functions that map indices p and q to new indices $\eta(p)$ and $\chi(q)$, respectively. We denote by $\boldsymbol{\sigma}_k(\cdot)$ the vector shift operator that shifts all vectors entries by k positions, i.e. if $v = (v_p)_p$, then $\boldsymbol{\sigma}_k(v) = (v_{p-k})_p$, and we denote by $\boldsymbol{\Sigma}_k(\cdot)$ the matrix shift operator that shifts all matrix entries by k positions parallel to the main diagonal of the matrix, i.e. if $M = (M_{pq})_{pq}$, then $\boldsymbol{\Sigma}_k(M) = (M_{p-k,q-k})_{pq}$. The symbols $\otimes$ and $\odot$ represent, respectively, the convolution operator of two vectors, and the component-wise product of two vectors or matrices. We denote by $\mathbb{E}[\cdot]$ the expectation operator, by $\Re\{\cdot\}$ the real-part operator, by $|\cdot|$ the absolute value, and by $[\![n,m]\!]$ the set of integers between n and m, where $n \leq m$. We denote by $\langle x,y\rangle = x^H y$ the hermitian scalar product, by $\langle x,y\rangle_{\Re} = \Re\{\langle x,y\rangle\}$ the real scalar product, and by $\|x\| = \sqrt{\langle x,x\rangle} = \sqrt{\langle x,x\rangle_{\Re}}$ the norm of x. Finally, we denote by mod the modulo operator.

II. SYSTEM MODEL

In this section, we consider the general FBMC system model on which this work is based, in its discrete-time version. For FBMC/QAM, the number of samples per symbol period is $N = Q$ for critical density systems, whereas it is $N = Q + N_g$ for non critical density systems, where Q is the number of subcarriers and N_g is the size of the CP interval. For FBMC/OQAM, the number of samples per symbol period is $N = Q/2$. For both QAM and OQAM, we denote by T the FBMC symbol period, by F the frequency separation between adjacent subcarriers, by FT the time-frequency occupancy of each transmitted symbol, and by $\Delta = 1/FT$ the lattice density. We denote by $T_s = 1/QF$ the sampling period and by $R_s = 1/T_s$ the sampling rate.

The FBMC transmitted signal can be expressed as

$$e = \sum_{m,n} a_{mn}\boldsymbol{\varphi}_{mn}, \tag{1}$$

where $m,n \in \mathbb{Z}$, a_{mn} is the data symbol transmitted at time nT and frequency mF, and

$$\boldsymbol{\varphi}_{mn} = e^{j\theta_{mn}}\left(\varphi_{q-nN}\right)_q \odot \left(e^{j2\pi mq/Q}\right)_q \tag{2}$$

refers to the phase, time and frequency shifted version of the transmitter prototype waveform, $\boldsymbol{\varphi} = (\varphi_q)_q$, used to transmit symbol a_{mn}. We point out that all signals could be seen as vectors in a space of infinite dimension in $\mathbb{C}$ and that transmitted symbols contributions span finite dimensions of this space (the number of which is given by the support of the Tx waveform). To make the system implementable, we assume that the supports durations, of both Tx/Rx waveforms, are finite and given by $D_{\boldsymbol{\varphi}}T$, where $D_{\boldsymbol{\varphi}}$ is the number of period in support duration. The phase shift θ_{mn} is used in FBMC/OQAM to guarantee the orthogonality between their in-phase and quadrature phase components counterparts in FBMC/QAM with respect to the real scalar product $\langle .,.\rangle_{\Re}$. In practice, we take $\theta_{mn} = (m+n)\,\pi/2$, for FBMC/OQAM, and $\theta_{mn} = 0$, for FBMC/QAM.

We consider a WSSUS channel [25] with a finite number of paths, L, and a channel impulse response (CIR) equal to

$$c(p;q) = \sum_{k=0}^{L-1} c_k e^{j2\pi\nu_k T_s q}\delta(p - p_k), \tag{3}$$

where c_k, ν_k and p_k are, respectively, the amplitude, frequency Doppler shift and time delay shift of the k^{th} path at time qT_s. The paths amplitudes c_k, $k = 0,\ldots,L-1$, are assumed to be centered and uncorrelated random complex Gaussian variables with average powers $\pi_k = \mathbb{E}[|c_k|^2]$.

The received signal is given by

$$r = \sum_{m,n} a_{mn}\tilde{\boldsymbol{\varphi}}_{mn} + n, \tag{4}$$

where $\tilde{\boldsymbol{\varphi}}_{mn}$ is the channel-distorted version of $\boldsymbol{\varphi}_{mn}$, seen at the receiver, with q^{th} element $\left[\tilde{\boldsymbol{\varphi}}_{mn}\right]_q = \sum_{k=0}^{L-1} c(p_k;q)\left[\boldsymbol{\varphi}_{mn}\right]_{q-p_k}$, and $n = (n_q)_q$ is a discrete-time base-band complex additive white Gaussian noise (AWGN) with zero mean and N_0 as variance, where $N_0/2$ is the two-sided power spectral density (PSD) of the continuous-time noise in the channel.

III. DERIVATION OF THE EXPRESSIONS OF USEFUL, INTERFERENCE AND NOISE POWERS

In this section, we derive the expressions of useful, interference and noise powers of both FBMC/OQAM and FBMC/QAM systems, using the same propagation channel conditions and by following the same steps as in [7].

A. FBMC/OQAM SYSTEMS

The decision variable on symbol a_{kl}, in (1), is given by

$$\Lambda_{kl} = \left\langle e^{\chi_{kl}}\boldsymbol{\psi}_{kl}, r\right\rangle_{\Re}, \tag{5}$$

where $\boldsymbol{\psi}_{kl} = e^{j\theta_{kl}}\left(\psi_{q-lN}\right)_q \odot \left(e^{j2\pi kq/Q}\right)_q$ is the phase, time and frequency shifted version of the receive prototype waveform, $\boldsymbol{\psi} = (\psi_q)_q$, used for the demodulation of the real symbol a_{kl}, with $D_{\boldsymbol{\psi}}$ the number of period in its finite support duration. We note that for simplification reasons, we assume that $D_{\boldsymbol{\varphi}} = D_{\boldsymbol{\psi}} = D$. We note that $D = D_{\text{OQAM}}/2 = D_{\text{QAM}}$, where D_{OQAM} and D_{QAM} are the number of period in the support duration for FBMC/OQAM and FBMC/QAM systems, respectively. The phase χ_{kl} is used to compensate, even partially, for the phase shift incurred by the channel at time-frequency location, (lT, kF), occupied by a_{kl}. Since the statistical characteristics of the decision variables are invariant by time and frequency translations within the time-frequency lattice of critical density, we can, without loss of generality, focus on the evaluation of the SINR for

symbol a_{00}, at time-frequency location $(0,0)$. The decision variable on a_{00} can be expanded into three terms, as

$$\Lambda_{00} = \underbrace{a_{00}\left\langle e^{j\chi_{00}}\boldsymbol{\psi}_{00}, \tilde{\boldsymbol{\varphi}}_{00}\right\rangle_{\Re}}_{U_{00}} + \underbrace{\sum_{\substack{m,n \\ (m,n)\neq(0,0)}} a_{mn}\left\langle e^{j\chi_{00}}\boldsymbol{\psi}_{00}, \tilde{\boldsymbol{\varphi}}_{mn}\right\rangle_{\Re}}_{I_{00}} + \underbrace{\left\langle e^{j\chi_{00}}\boldsymbol{\psi}_{00}, n\right\rangle_{\Re}}_{N_{00}}, \quad (6)$$

where U_{00}, I_{00} and N_{00} are the useful, interference and noise terms, respectively.

We start by deriving the useful and interference powers, and we will study the noise power later. The useful and interference powers must be averaged with respect to the channel realizations, the modulated signal (so of the realizations of the transmitted sequences a_{mn}) and the noise. These powers depend only on the realizations of the transmitted signal and the channel. Thus, we start by averaging with respect to the realizations of the transmitted signal, conditionally to any realization of the channel, then with respect to the realizations of the channel. Conditional on a given realization of the CIR, $c(p;q)$, the average powers of the useful and interference terms are given by

$$\begin{cases} P_U^c = \mathbb{E}\left[U_{00}^2\right] = \mathbb{E}\left[a_{00}^2\right]\left(\Re\left\{e^{-j\chi_{00}}\left\langle\boldsymbol{\psi}_{00}, \tilde{\boldsymbol{\varphi}}_{00}\right\rangle\right\}\right)^2, \\ P_I^c = \mathbb{E}\left[I_{00}^2\right] = \sum\limits_{\substack{m,n \\ (m,n)\neq(0,0)}} \mathbb{E}\left[a_{mn}^2\right]\left(\Re\left\{e^{-j\chi_{00}}\left\langle\boldsymbol{\psi}_{00}, \tilde{\boldsymbol{\varphi}}_{mn}\right\rangle\right\}\right)^2. \end{cases} \quad (7)$$

The interference term in (7) results from the uncorrelated nature of the real transmitted symbols, a_{mn}. The average transmitted energy corresponding to real symbol a_{mn} is given by $E_s = \mathbb{E}\left[\|a_{mn}\boldsymbol{\varphi}\|^2\right] = \mathbb{E}\left[a_{mn}^2\right]\|\boldsymbol{\varphi}\|^2$, which is equivalent to have $\mathbb{E}\left[a_{mn}^2\right] = \frac{E_s}{\|\boldsymbol{\varphi}\|^2}$.

To calculate the SINR, an averaging over the channel realizations is needed. To simplify the optimization problem, we can use the transfer function of the channel, $C(f;q) = \sum_{k=0}^{L-1} c_k e^{j2\pi\nu_k T_s q} e^{-j2\pi p_k T_s f}$, which is the Fourier transform of the CIR, $c(p;q)$, with respect to p, and choose the compensation factor,

$$e^{j\chi_{00}} = \frac{C(0;0)}{|C(0;0)|} = \frac{\sum\limits_{l=0}^{L-1} c_l}{\left|\sum\limits_{k=0}^{L-1} c_k\right|}. \quad (8)$$

By averaging the expressions in (7) over the channel realizations, the useful and interference powers are, respectively, given by

$$\begin{cases} P_U = \mathbb{E}\left[P_U^c\right] = \dfrac{E_s}{\|\varphi\|^2}\mathbb{E}\left[\left(\Re\left\{e^{-j\chi_{00}}\left\langle\boldsymbol{\psi}_{00}, \tilde{\boldsymbol{\varphi}}_{00}\right\rangle\right\}\right)^2\right], \\ P_I = \mathbb{E}\left[P_I^c\right] = \dfrac{E_s}{\|\varphi\|^2}\sum\limits_{\substack{m,n \\ (m,n)\neq(0,0)}} \mathbb{E}\left[\left(\Re\left\{e^{-j\chi_{00}}\left\langle\boldsymbol{\psi}_{00}, \tilde{\boldsymbol{\varphi}}_{mn}\right\rangle\right\}\right)^2\right]. \end{cases} \quad (9)$$

Let $\overline{E}_s = E_s\sum_{k=0}^{L-1}\pi_k$ be the average energy received per real symbol, and $\tilde{\pi}_k = \pi_k \Big/ \sum_{k=0}^{L-1}\pi_k$ be the normalized multipath power profile of the channel. From (A.13) in Appendix A, we deduce that

$$\begin{aligned} P_U = {} & \frac{\overline{E}_s}{2\|\boldsymbol{\varphi}\|^2} \\ & \times\left(\begin{array}{l} \Re\left\{\boldsymbol{\psi}^H\left[\begin{array}{l}\left(\sum\limits_{k=0}^{L-1}\tilde{\pi}_k\boldsymbol{\xi}_{\nu_k}\odot\boldsymbol{\sigma}_{p_k}(\boldsymbol{\varphi})\right) \\ \times\left(\sum\limits_{l=0}^{L-1}\tilde{\pi}_l\boldsymbol{\xi}_{\nu_l}\odot\boldsymbol{\sigma}_{p_l}(\boldsymbol{\varphi})\right)^T\end{array}\right]\boldsymbol{\psi}^*\right\} \\ +\boldsymbol{\psi}^H\left[\sum\limits_{k=0}^{L-1}\tilde{\pi}_k\boldsymbol{\Phi}_{\nu_k}\odot\left(\boldsymbol{\sigma}_{p_k}(\boldsymbol{\varphi})\boldsymbol{\sigma}_{p_k}(\boldsymbol{\varphi})^H\right)\right]\boldsymbol{\psi}\end{array}\right), \\ P_I = {} & \frac{\overline{E}_s}{2\|\boldsymbol{\varphi}\|^2}\sum_{\substack{m,n \\ (m,n)\neq(0,0)}} \\ & \times\left(\begin{array}{l} \Re\left\{\boldsymbol{\psi}^H\left[\begin{array}{l}\left(\sum\limits_{k=0}^{L-1}\tilde{\pi}_k\boldsymbol{\xi}_{\nu_k}\odot\boldsymbol{\sigma}_{p_k}(\boldsymbol{\varphi}_{mn})\right) \\ \times\left(\sum\limits_{l=0}^{L-1}\tilde{\pi}_l\boldsymbol{\xi}_{\nu_l}\odot\boldsymbol{\sigma}_{p_l}(\boldsymbol{\varphi}_{mn})\right)^T\end{array}\right]\boldsymbol{\psi}^*\right\} \\ +\boldsymbol{\psi}^H\sum\limits_{k=0}^{L-1}\left(\begin{array}{l}\tilde{\pi}_k\boldsymbol{\Phi}_{\nu_k} \\ \odot\left(\boldsymbol{\sigma}_{p_k}(\boldsymbol{\varphi}_{mn})\boldsymbol{\sigma}_{p_k}(\boldsymbol{\varphi}_{mn})^H\right)\end{array}\right)\boldsymbol{\psi}\end{array}\right), \end{aligned} \quad (10)$$

where $\boldsymbol{\xi}_\nu$ is the complex vector defined as $\left(\boldsymbol{\xi}_\nu\right)_q = \left(e^{j2\pi\nu T_s q}\right)_q$, $\boldsymbol{\Phi}_\nu$ is the Hermitian matrix defined as $(\boldsymbol{\Phi}_\nu)_{pq} = \left(e^{j2\pi\nu T_s(p-q)}\right)_{pq}$, and $\boldsymbol{\sigma}_k(\cdot)$ is the vector shift operator.

The noise power is expressed as

$$P_N = \mathbb{E}\left[\left(\Re\left\{e^{-j\chi_{00}}\left\langle\boldsymbol{\psi}_{00}, n\right\rangle\right\}\right)^2\right]. \quad (11)$$

The term $\left\langle\boldsymbol{\psi}_{00}, n\right\rangle$ is independent of $e^{-j\chi_{00}}$, which depends directly on the channel realizations that are independent of the noise. In fact, $\left\langle\boldsymbol{\psi}_{00}, n\right\rangle$ is a Gaussian complex random variable whose statistical properties remain unchanged with a phase shift such as $e^{-j\chi_{00}}$. Thus, $e^{-j\chi_{00}}\left\langle\boldsymbol{\psi}_{00}, n\right\rangle$ is a circular random complex Gaussian variable that has the same variance as $\left\langle\boldsymbol{\psi}_{00}, n\right\rangle$. Therefore, $\Re\left\{e^{-j\chi_{00}}\left\langle\boldsymbol{\psi}_{00}, n\right\rangle\right\}$ is a random real Gaussian variable with the half variance of $\left\langle\boldsymbol{\psi}_{00}, n\right\rangle$. Consequently, the noise power can be written as

$$P_N = \frac{1}{2}\mathbb{E}\left[\left|\left\langle\boldsymbol{\psi}_{00}, n\right\rangle\right|^2\right]. \quad (12)$$

Since the noise is white, with autocorrelation matrix $R_{nn} = N_0 I$, where I is the infinite dimensions identity matrix, we can write

$$\mathbb{E}\left[\left|\langle\boldsymbol{\psi}, n\rangle\right|^2\right] = \boldsymbol{\psi}^H\underbrace{\mathbb{E}\left[nn^H\right]}_{R_{nn}=N_0 I}\boldsymbol{\psi}, = N_0\|\boldsymbol{\psi}\|^2. \quad (13)$$

Accordingly, the noise power is given by

$$P_N = \frac{N_0}{2}\|\boldsymbol{\psi}\|^2. \quad (14)$$

B. FBMC/QAM SYSTEMS

The SINR expression for FBMC/QAM systems was derived in [23], in the discrete-time context. In this section, we briefly present the main steps considered to find its closed-form expression.

The decision variable on complex symbol a_{kl}, bearing simultaneously both in-phase and quadrature phase components, uses the conventional Hermitian scalar product, and can be expressed as

$$\Lambda_{kl} = \langle \boldsymbol{\psi}_{kl}, r \rangle, \tag{15}$$

where $\boldsymbol{\psi}_{kl} = \left(\psi_{q-nN}\right)_q \odot \left(e^{j2\pi mq/Q}\right)_q$ is the time and frequency shifted version of the receiver prototype waveform, $\boldsymbol{\psi} = \left(\psi_q\right)_q$, used for the demodulation of the complex symbol a_{kl}.

As in FBMC/OQAM, we evaluate, without loss of generality, the SINR for symbol a_{00}. The decision variable on a_{00} can also be expanded into three terms as

$$\Lambda_{00} = \underbrace{a_{00}\langle \boldsymbol{\psi}_{00}, \tilde{\boldsymbol{\varphi}}_{00} \rangle}_{U_{00}} + \underbrace{\sum_{\substack{m,n \\ (m,n)\neq(0,0)}} a_{mn}\langle \boldsymbol{\psi}_{00}, \tilde{\boldsymbol{\varphi}}_{mn} \rangle}_{I_{00}} + \underbrace{\langle \boldsymbol{\psi}_{00}, n \rangle}_{N_{00}}, \tag{16}$$

where U_{00}, I_{00} and N_{00} are the useful, interference and noise terms, respectively.

Conditional on a given realization of the CIR, $c(p;q)$, the average powers of the useful and interference terms are given by

$$\begin{cases} P_U^c = \mathbb{E}\left[U_{00}^2\right] = \mathbb{E}\left[a_{00}^2\right]\left|\langle \boldsymbol{\psi}_{00}, \tilde{\boldsymbol{\varphi}}_{00} \rangle\right|^2, \\ P_I^c = \mathbb{E}\left[I_{00}^2\right] = \sum\limits_{\substack{m,n \\ (m,n)\neq(0,0)}} \mathbb{E}\left[a_{mn}^2\right]\left|\langle \boldsymbol{\psi}_{00}, \tilde{\boldsymbol{\varphi}}_{mn} \rangle\right|^2. \end{cases} \tag{17}$$

Let E be the mean energy of complex symbol a_{mn}. Then, for comparison purposes and since we transmit separately the in-phase and quadrature phase components in the case of FBMC/OQAM, we assume that $E = 2E_s$, which means that $\mathbb{E}\left[a_{mn}^2\right] = \frac{E}{2\|\boldsymbol{\varphi}\|^2}$. We re-iterate the same reasoning as in Section III-A, we conclude that

$$\begin{cases} P_U = \dfrac{E}{\|\boldsymbol{\varphi}\|^2}\mathbb{E}\left[\left|\langle \boldsymbol{\psi}_{00}, \tilde{\boldsymbol{\varphi}}_{00} \rangle\right|^2\right], \\ P_I = \dfrac{E}{\|\boldsymbol{\varphi}\|^2} \sum\limits_{\substack{mn \\ (m,n)\neq(0,0)}} \mathbb{E}\left[\left|\langle \boldsymbol{\psi}_{00}, \tilde{\boldsymbol{\varphi}}_{mn} \rangle\right|^2\right]. \end{cases} \tag{18}$$

Let $\overline{E} = E\sum_{k=0}^{L-1}\pi_k$ be the average energy received per complex symbol, and $\tilde{\pi}_k = \pi_k \Big/ \sum_{k=0}^{L-1}\pi_k$ be the normalized multipath power profile of the channel. The useful and the interference powers can be written as

$$\begin{cases} P_U = \dfrac{\overline{E}}{\|\boldsymbol{\varphi}\|^2}\boldsymbol{\psi}^H\left[\sum\limits_{k=0}^{L-1}\tilde{\pi}_k\boldsymbol{\Phi}_{\nu_k} \odot \left(\boldsymbol{\sigma}_{p_k}(\boldsymbol{\varphi})\,\boldsymbol{\sigma}_{p_k}(\boldsymbol{\varphi})^H\right)\right]\boldsymbol{\psi}, \\ P_I = \dfrac{\overline{E}}{\|\boldsymbol{\varphi}\|^2} \\ \qquad \sum\limits_{\substack{mn \\ (m,n)\neq(0,0)}} \boldsymbol{\psi}^H\left[\begin{array}{l}\sum\limits_{k=0}^{L-1}\tilde{\pi}_k\boldsymbol{\Phi}_{\nu_k} \\ \odot\left(\boldsymbol{\sigma}_{p_k}(\boldsymbol{\varphi}_{mn})\,\boldsymbol{\sigma}_{p_k}(\boldsymbol{\varphi}_{mn})^H\right)\end{array}\right]\boldsymbol{\psi}. \end{cases} \tag{19}$$

The noise power is given by

$$P_N = \mathbb{E}\left[\left|\langle \boldsymbol{\psi}_{00}, n \rangle\right|^2\right] = N_0\|\boldsymbol{\psi}\|^2. \tag{20}$$

In the next section, we will use the obtained expressions of the useful, interference and noise powers to derive the SINR.

IV. SINR EXPRESSION

The SINR expression is the following

$$\text{SINR} = \frac{P_S}{P_I + P_N}. \tag{21}$$

We inject in (21) the expressions in (10) and (14), for FBMC/OQAM, and in (19) and (20), for FBMC/QAM.

In the sequel, we choose using real waveforms, since this choice extremely simplifies the equations for FBMC/OQAM, without affecting much their performance. This choice also allows to compact the expressions for FBMC/QAM, as the optimization shows that the optimal waveforms obtained for these systems are real, with a term of close phase. In this case, the SINR can be expressed as

$$\text{SINR} = \frac{\boldsymbol{\psi}^T M_{00}^{\boldsymbol{\varphi}}\boldsymbol{\psi}}{\boldsymbol{\psi}^T\left(\sum\limits_{\substack{m,n \\ (m,n)\neq(0,0)}} M_{mn}^{\boldsymbol{\varphi}} + (1+\gamma)\frac{N_0}{E}\|\boldsymbol{\varphi}\|^2\right)\boldsymbol{\psi}}, \tag{22}$$

where

$$M_{mn}^{\boldsymbol{\varphi}} = \Re\left\{\begin{array}{l}\sum\limits_{k=0}^{L-1}\tilde{\pi}_k\boldsymbol{\Phi}_{\nu_k} \odot \left(\boldsymbol{\sigma}_{p_k}(\boldsymbol{\varphi}_{mn})\,\boldsymbol{\sigma}_{p_k}(\boldsymbol{\varphi}_{mn})^H\right) \\ +\gamma\left(\sum\limits_{k=0}^{L-1}\tilde{\pi}_k\boldsymbol{\xi}_{\nu_k} \odot \boldsymbol{\sigma}_{p_k}(\boldsymbol{\varphi}_{mn})\right) \\ \times\left(\sum\limits_{l=0}^{L-1}\tilde{\pi}_l\boldsymbol{\xi}_{\nu_l} \odot \boldsymbol{\sigma}_{p_l}(\boldsymbol{\varphi}_{mn})\right)^T\end{array}\right\},$$

$\gamma = 1$ for FBMC/OQAM, and $\gamma = 0$ for FBMC/QAM.

To simplify derivations, we introduce the matrix

$$M_{\infty}^{\boldsymbol{\varphi}} = \sum_{mn} M_{mn}^{\boldsymbol{\varphi}} = M_{00}^{\boldsymbol{\varphi}} + \sum_{\substack{mn \\ (m,n)\neq(0,0)}} M_{mn}^{\boldsymbol{\varphi}}. \tag{23}$$

Therefore, the expression of the SINR can be written as

$$\text{SINR} = \frac{\boldsymbol{\psi}^T M_{00}^{\boldsymbol{\varphi}}\boldsymbol{\psi}}{\boldsymbol{\psi}^T\left(M_{\infty}^{\boldsymbol{\varphi}} - M_{00}^{\boldsymbol{\varphi}} + (1+\gamma)\frac{N_0}{E}\|\boldsymbol{\varphi}\|^2\right)\boldsymbol{\psi}}, \tag{24}$$

where $M_{00}^{\boldsymbol{\varphi}}$ and $M_{\infty}^{\boldsymbol{\varphi}}$ are, respectively, given by

$$M_{00}^{\boldsymbol{\varphi}} = \Re\left\{\begin{array}{l}\left(\sum_{k=0}^{L-1}\tilde{\pi}_k\boldsymbol{\Phi}_{\nu_k}\odot\boldsymbol{\Sigma}_{p_k}\left(\boldsymbol{\varphi}\boldsymbol{\varphi}^T\right)\right)\\ +\gamma\left(\sum_{k=0}^{L-1}\tilde{\pi}_k\boldsymbol{\xi}_{\nu_k}\odot\boldsymbol{\sigma}_{p_k}(\boldsymbol{\varphi})\right)\\ \times\left(\sum_{l=0}^{L-1}\tilde{\pi}_l\boldsymbol{\xi}_{\nu_l}\odot\boldsymbol{\sigma}_{p_l}(\boldsymbol{\varphi})\right)^T\end{array}\right\} \tag{25}$$

and

$$M_{\infty}^{\boldsymbol{\varphi}} = \Re\left\{\begin{array}{l}\left(\sum_{k=0}^{L-1}\tilde{\pi}_k\boldsymbol{\Phi}_{\nu_k}\odot\sum_n\boldsymbol{\Sigma}_{p_k+nN}\left(\boldsymbol{\varphi}\boldsymbol{\varphi}^T\right)\right)\\ \odot\left(\sum_{m=0}^{Q-1}\boldsymbol{\Phi}_{m/QT_s}\right)\\ +\gamma\sum_n\left[\begin{array}{l}(-1)^n\left(\sum_{k=0}^{L-1}\tilde{\pi}_k\boldsymbol{\xi}_{\nu_k}\odot\boldsymbol{\sigma}_{p_k+nN}(\boldsymbol{\varphi})\right)\\ \times\left(\sum_{l=0}^{L-1}\tilde{\pi}_l\boldsymbol{\xi}_{\nu_l}\odot\boldsymbol{\sigma}_{p_l+nN}(\boldsymbol{\varphi})\right)^T\end{array}\right]\\ \odot\left(\sum_{m=0}^{Q-1}(-1)^m\boldsymbol{\sigma}_{p_k}\left(\boldsymbol{\xi}_{m/QT_s}\right)\boldsymbol{\sigma}_{p_l}\left(\boldsymbol{\xi}_{m/QT_s}\right)^T\right)\end{array}\right\}, \tag{26}$$

with $\boldsymbol{\Sigma}_k(\cdot)$ is the matrix shift operator,

$$\left[\sum_{m=0}^{Q-1}\boldsymbol{\Phi}_{m/QT_s}\right]_{pq} = \begin{cases}Q, & \text{if } (p-q) \bmod (Q) = 0,\\ 0, & \text{else,}\end{cases} \tag{27}$$

and

$$\left[\sum_{m=0}^{Q-1}(-1)^m\boldsymbol{\sigma}_{p_k}\left(\boldsymbol{\xi}_{m/QT_s}\right)\boldsymbol{\sigma}_{p_l}\left(\boldsymbol{\xi}_{m/QT_s}\right)^T\right]_{pq} = \begin{cases}Q, & \text{if } (p+q-p_k-p_l) \bmod (Q) = \dfrac{Q}{2},\\ 0, & \text{else.}\end{cases} \tag{28}$$

Using the expressions in (24), (25), and (26), we deduce a second expression of the SINR as a ratio of two quadratic forms on $\boldsymbol{\varphi}$ as follows

$$\text{SINR} = \frac{\boldsymbol{\varphi}^T M_{00}^{\boldsymbol{\psi}}\boldsymbol{\varphi}}{\boldsymbol{\varphi}^T\left(M_{\infty}^{\boldsymbol{\psi}} - M_{00}^{\boldsymbol{\psi}} + (1+\gamma)\frac{N_0}{E}\|\boldsymbol{\psi}\|^2\right)\boldsymbol{\varphi}}, \tag{29}$$

where

$M_{\infty}^{\boldsymbol{\psi}}$

$$= \Re\left\{\begin{array}{l}\sum_{k=0}^{L-1}\tilde{\pi}_k\boldsymbol{\Phi}_{\nu_k}\odot\sum_n\boldsymbol{\Sigma}_{-p_k+nN}\left(\boldsymbol{\psi}\boldsymbol{\psi}^T\right)\odot\left(\sum_{m=0}^{Q-1}\boldsymbol{\Phi}_{m/QT_s}\right)\\ +\gamma\sum_n\left[\begin{array}{l}(-1)^n\\ \times\boldsymbol{\Sigma}_{nN}\left(\begin{array}{l}\left(\sum_{k=0}^{L-1}\tilde{\pi}_k\boldsymbol{\Sigma}_{-p_k}\left(\boldsymbol{\xi}_{\nu_k}\odot\boldsymbol{\psi}\right)\right)\\ \times\left(\sum_{l=0}^{L-1}\tilde{\pi}_l\boldsymbol{\Sigma}_{-p_l}\left(\boldsymbol{\xi}_{\nu_l}\odot\boldsymbol{\psi}\right)\right)^T\end{array}\right)\end{array}\right]\\ \odot\left(\sum_{m=0}^{Q-1}(-1)^m\boldsymbol{\xi}_{m/QT_s}\boldsymbol{\xi}_{m/QT_s}^T\right)\end{array}\right\} \tag{30}$$

and

$$M_{00}^{\boldsymbol{\psi}} = \Re\left\{\begin{array}{l}\left(\sum_{k=0}^{L-1}\tilde{\pi}_k\boldsymbol{\Phi}_{\nu_k}\odot\boldsymbol{\Sigma}_{-p_k}\left(\boldsymbol{\psi}\boldsymbol{\psi}^T\right)\right)\\ +\gamma\left(\sum_{k=0}^{L-1}\tilde{\pi}_k\boldsymbol{\Sigma}_{-p_k}\left(\boldsymbol{\xi}_{\nu_k}\odot\boldsymbol{\psi}\right)\right)\\ \times\left(\sum_{l=0}^{L-1}\tilde{\pi}_l\boldsymbol{\Sigma}_{-p_l}\left(\boldsymbol{\xi}_{\nu_l}\odot\boldsymbol{\psi}\right)\right)^T\end{array}\right\}. \tag{31}$$

In the sequel, we consider a diffuse scattering function in the frequency domain, with a Doppler spectral density, decoupled from the dispersion in the time domain, given by

$$\tilde{S}(l;\nu) = \alpha(\nu)\,\tilde{\beta}(l), \tag{32}$$

where $\alpha(\nu)$ is the Doppler specter density, and $\tilde{\beta}(l) = \sum_{k=0}^{L-1}\tilde{\pi}_k\delta(l-p_k)$, with $\tilde{\pi}_k$ is the total average power of all paths with common delay p_kT_s, and L is the total number of delays. In this case, we can rewrite the expressions in (25), (26), (30), and (31) in a more compact form as

$$M_{00}^{\boldsymbol{\varphi}} = \Re\left\{\begin{array}{l}\left(\sum_{k=0}^{L-1}\tilde{\pi}_k\boldsymbol{\Sigma}_{p_k}\left(\boldsymbol{\varphi}\boldsymbol{\varphi}^T\right)\right)\odot\boldsymbol{\Pi}\\ +\gamma\left(\sum_{k=0}^{L-1}\tilde{\pi}_k\boldsymbol{\sigma}_{p_k}(\boldsymbol{\varphi})\right)\left(\sum_{l=0}^{L-1}\tilde{\pi}_l\boldsymbol{\sigma}_{p_l}(\boldsymbol{\varphi})\right)^T\odot\boldsymbol{\eta}\boldsymbol{\eta}^T\end{array}\right\}, \tag{33}$$

$$M_{\infty}^{\boldsymbol{\varphi}} = \Re\left\{\begin{array}{l}\boldsymbol{\Omega}\odot\sum_n\boldsymbol{\Sigma}_{nN}\sum_{k=0}^{L-1}\tilde{\pi}_k\boldsymbol{\Sigma}_{p_k}\left(\boldsymbol{\varphi}\boldsymbol{\varphi}^T\right)\\ +\gamma\boldsymbol{\eta}\boldsymbol{\eta}^T\odot\\ \sum_n(-1)^n\boldsymbol{\Sigma}_{nN}\sum_{k,l=0}^{L-1}\left(\begin{array}{l}\tilde{\pi}_k\tilde{\pi}_l\boldsymbol{\Theta}^{(kl)}\\ \odot\left(\boldsymbol{\sigma}_{p_k}(\boldsymbol{\varphi})\boldsymbol{\sigma}_{p_l}(\boldsymbol{\varphi})^T\right)\end{array}\right)\end{array}\right\}, \tag{34}$$

$$M_{00}^{\boldsymbol{\psi}} = \Re\left\{\begin{array}{l}\left(\sum_{k=0}^{L-1}\tilde{\pi}_k\boldsymbol{\Sigma}_{-p_k}\left(\boldsymbol{\psi}\boldsymbol{\psi}^T\right)\right)\odot\boldsymbol{\Pi}\\ +\gamma\left(\sum_{k=0}^{L-1}\tilde{\pi}_k\boldsymbol{\sigma}_{-p_k}(\boldsymbol{\eta}\odot\boldsymbol{\psi})\right)\\ \times\left(\sum_{l=0}^{L-1}\tilde{\pi}_l\boldsymbol{\sigma}_{-p_l}(\boldsymbol{\eta}\odot\boldsymbol{\psi})\right)^T\end{array}\right\}, \tag{35}$$

$$M_{\infty}^{\boldsymbol{\psi}} = \Re\left\{\begin{array}{l}\boldsymbol{\Omega}\odot\sum\limits_{n}\boldsymbol{\Sigma}_{nN}\sum\limits_{k=0}^{L-1}\tilde{\pi}_k\boldsymbol{\Sigma}_{-p_k}\left(\boldsymbol{\psi}\boldsymbol{\psi}^T\right)\\ +\gamma\boldsymbol{\Theta}_2\\ \odot\sum\limits_{n}(-1)^n\boldsymbol{\Sigma}_{nN}\left[\begin{array}{l}\left(\sum\limits_{k=0}^{L-1}\tilde{\pi}_k\boldsymbol{\sigma}_{-p_k}(\boldsymbol{\eta}\odot\boldsymbol{\psi})\right)\\ \times\left(\sum\limits_{l=0}^{L-1}\tilde{\pi}_l\boldsymbol{\sigma}_{-p_l}(\boldsymbol{\eta}\odot\boldsymbol{\psi})\right)^T\end{array}\right]\end{array}\right\}, \tag{36}$$

where the vector $\boldsymbol{\eta}$ and the matrices $\boldsymbol{\Pi}$, $\boldsymbol{\Omega}$, $\boldsymbol{\Theta}^{(kl)}$, and $\boldsymbol{\Theta}_2$ are defined as

$$\left\{\begin{array}{l}\boldsymbol{\eta}=\int\alpha(\nu)\boldsymbol{\xi}_\nu d\nu,\\ \boldsymbol{\Pi}=\int\alpha(\nu)\boldsymbol{\Phi}_\nu d\nu,\\ \boldsymbol{\Omega}=\left(\int\alpha(\nu)\boldsymbol{\Phi}_\nu d\nu\right)\odot\left(\sum\limits_{m=0}^{Q-1}\boldsymbol{\Phi}_{m/QT_s}\right),\\ \boldsymbol{\Theta}^{(kl)}=\sum\limits_{m=0}^{Q-1}(-1)^m\boldsymbol{\sigma}_{p_k}\left(\boldsymbol{\xi}_{m/QT_s}\right)\boldsymbol{\sigma}_{p_l}\left(\boldsymbol{\xi}_{m/QT_s}\right)^T,\\ \boldsymbol{\Theta}_2=\sum\limits_{m=0}^{Q-1}(-1)^m\boldsymbol{\xi}_{m/QT_s}\boldsymbol{\xi}_{m/QT_s}^T.\end{array}\right. \tag{37}$$

The $(p,q)^{\text{th}}$ entries of the matrices $\boldsymbol{\Omega}$, $\boldsymbol{\Theta}^{(kl)}$, and $\boldsymbol{\Theta}_2$ can be, respectively, written in a simpler way as

$$\left\{\begin{array}{l}\Omega_{pq}=\begin{cases}Q\Pi_{pq}, & \text{if } (p-q) \bmod (Q)=0,\\ 0, & \text{else,}\end{cases}\\ \left[\boldsymbol{\Theta}^{(kl)}\right]_{pq}=\begin{cases}Q, & \text{if } (p+q-p_k-p_l) \bmod (Q)=\dfrac{Q}{2},\\ 0, & \text{else,}\end{cases}\\ \left[\boldsymbol{\Theta}_2\right]_{pq}=\begin{cases}Q, & \text{if } (p+q) \bmod (Q)=\dfrac{Q}{2},\\ 0, & \text{else.}\end{cases}\end{array}\right. \tag{38}$$

We note that the expressions of generalized Rayleigh ratios that allow to optimize $\boldsymbol{\varphi}$ for a given $\boldsymbol{\psi}$, and $\boldsymbol{\psi}$ for a given $\boldsymbol{\varphi}$, are not symmetrical in FBMC/OQAM systems, unlike the FBMC/QAM ones. This makes the implementation of these equations more difficult in FBMC/OQAM.

To preserve the same notations used in the continuous-time, we can rewrite the SINR as

$$\text{SINR}=\frac{\boldsymbol{\psi}^T A_{\boldsymbol{\varphi}}\boldsymbol{\psi}}{\boldsymbol{\psi}^T B_{\boldsymbol{\varphi}}\boldsymbol{\psi}}, \tag{39}$$

where $A_{\boldsymbol{\varphi}}=M_{00}^{\boldsymbol{\varphi}}$ and $B_{\boldsymbol{\varphi}}=M_{\infty}^{\boldsymbol{\varphi}}-M_{00}^{\boldsymbol{\varphi}}+(1+\gamma)\frac{N_0}{E}\|\boldsymbol{\varphi}\|^2$, or as

$$\text{SINR}=\frac{\boldsymbol{\varphi}^T A_{\boldsymbol{\psi}}\boldsymbol{\varphi}}{\boldsymbol{\varphi}^T B_{\boldsymbol{\psi}}\boldsymbol{\varphi}}, \tag{40}$$

where $A_{\boldsymbol{\psi}}=M_{00}^{\boldsymbol{\psi}}$ and $B_{\boldsymbol{\psi}}=M_{\infty}^{\boldsymbol{\psi}}-M_{00}^{\boldsymbol{\psi}}+(1+\gamma)\frac{N_0}{E}\|\boldsymbol{\psi}\|^2$.

V. POPS OPTIMIZATION ALGORITHM

The resulting optimization problem is defined as

$$\left(\boldsymbol{\varphi}_{opt},\boldsymbol{\psi}_{opt}\right)=\arg\max_{(\boldsymbol{\varphi},\boldsymbol{\psi})}\text{SINR}. \tag{41}$$

Given the special forms of the SINR expressions in (39) and (40), it is easy to see that the optimization problem is equivalent to a maximization of a generalized Rayleigh quotient. For finite values of the SNR, $\frac{N_0}{E}$ is non-null, and $\frac{N_0}{E}\|\boldsymbol{\varphi}\|^2$ and $\frac{N_0}{E}\|\boldsymbol{\psi}\|^2$ are trivial quadratic forms which, when added to the positive Hermitian quadratic forms in the expressions of $\boldsymbol{B}_{\boldsymbol{\varphi}}$ and $B_{\boldsymbol{\psi}}$, guarantee their invertibility and their relative well-conditioning.

Algorithm 1 POPS Algorithm in the Discrete-Time Systems

Require: SNR, B_dT_m, L, Q, D, FT, $F=1$, $T_s=1/Q$, $\boldsymbol{\varphi}^{(0)}$, $\text{SINR}^{(0)}$, $i=0$, $e_{\text{SINR}}=1$ and $\varepsilon=10^{-7}$

1: Compute B_d and T_m for given B_dT_m and L.
2: Compute $\boldsymbol{\eta}$, $\boldsymbol{\Pi}$, and $\boldsymbol{\Omega}$ for given $\alpha(\nu)$.
3: Compute $\boldsymbol{\Theta}_2$.
4: **while** $e_{\text{SINR}}>\varepsilon$ **do**
5: Compute $A_{\boldsymbol{\varphi}}^{(i)}$ and $B_{\boldsymbol{\varphi}}^{(i)}$.
6: Compute $G_{\boldsymbol{\varphi}}^{(i)}=\left(B_{\boldsymbol{\varphi}}^{(i)}\right)^{-1}A_{\boldsymbol{\varphi}}^{(i)}$.
7: Calculate $\left[\boldsymbol{\psi}^{(i)},\lambda_{1\max}^{(i)}\right]=eig\left(G_{\boldsymbol{\varphi}}^{(i)}\right)$.
8: Compute $A_{\boldsymbol{\psi}}^{(i)}$ and $B_{\boldsymbol{\psi}}^{(i)}$.
9: Compute $G_{\boldsymbol{\psi}}^{(i)}=\left(B_{\boldsymbol{\psi}}^{(i)}\right)^{-1}A_{\boldsymbol{\psi}}^{(i)}$.
10: Calculate $\left[\boldsymbol{\varphi}^{(i)},\lambda_{2\max}^{(i)}\right]=eig\left(G_{\boldsymbol{\psi}}^{(i)}\right)$.
11: $i\leftarrow i+1$
12: $\text{SINR}^{(i)}\leftarrow\lambda_{2\max}$
13: Evaluate errors: $e_{\text{SINR}}=\left|\text{SINR}^{(i)}-\text{SINR}^{(i-1)}\right|$.
14: **end while**

The POPS approach, proposed to optimize the Tx/Rx waveforms, is detailed in **Algorithm 1**, where B_d and T_m are, respectively, the Doppler spread and the delay spread,

$$\alpha(\nu)=\begin{cases}\dfrac{\delta}{B_d}+\dfrac{2(1-\delta)}{\pi B_d\sqrt{1-(2\nu/B_d)^2}}, & \text{if } |\nu|<\dfrac{B_d}{2}\\ 0, & \text{else,}\end{cases} \tag{42}$$

and

$$\beta(l)=\begin{cases}\dfrac{\delta lT_s}{T_m}+\dfrac{(1-\delta)\,e^{-lT_s/T_m}}{T_m}, & \text{if } |l|\le\dfrac{L-1}{2}\\ 0, & \text{else,}\end{cases} \tag{43}$$

where $\delta=1$ for the uniform distribution for the channel multipath power profile, $\beta(l)$, and the uniform Doppler specter density, $\alpha(\nu)$, and $\delta=0$ for the exponential truncated decaying model, $\beta(l)$, and the classic Doppler specter density, $\alpha(\nu)$, (i.e. Jakes model). In the sequel, we denote by the first channel "the uniform channel", and the second channel "the exponential channel".

The main steps of the POPS approach **(Algorithm 1)** are the following:

- **Step 1:** We compute the matrices $\boldsymbol{\eta}$, $\boldsymbol{\Pi}$, and $\boldsymbol{\Omega}$ for given α (ν).
- **Step 2:** We compute the matrix $\boldsymbol{\Theta}_2$.
- **Step 3:** In the initialization step of **Algorithm 1**, we start by an arbitrary non null vector $\boldsymbol{\varphi}^{(0)}$, typically the Gaussian function.
- **Step 4:** For iteration (i) , we compute $\boldsymbol{\psi}^{(i)}$ as the eigenvector of $G_{\boldsymbol{\varphi}}^{(i)}$ with maximum eigenvalue, $\lambda_{1\max}^{(i)}$.
- **Step 5:** Given $\boldsymbol{\psi}^{(i)}$, we determine $\boldsymbol{\varphi}^{(i)}$ as the eigenvector of $G_{\boldsymbol{\psi}}^{(i)}$ with maximum eigenvalue, $\lambda_{2\max}^{(i)}$.
- **Step 6:** We proceed to the next iteration, $(i+1)$.
- **Step 7:** We stop the iterations when we obtain a negligible increase of SINR.

In the next section, we will consider this algorithm and analyze the performance of the optimal obtained waveforms.

VI. SIMULATION RESULTS

In this section, we assess the performance of discrete-time FBMC/OQAM systems, in terms of achieved SINR and OOB emissions. Subsequently, we compare these performances with those of discrete-time FBMC/QAM and continuous-time FBMC/OQAM. It is very important to compare the discrete-time and continuous-time versions of FBMC/OQAM, since the ways to explore the signal spaces are different. We report that in continuous-time context, we use the Hermite functions in finite numbers to explore a part of the infinite space of square-integrable function, while in discrete-time context, we explore the entire space of finite dimensions that represents the samples number of the optimized waveforms support.

A. FBMC/OQAM SYSTEMS PERFORMANCE

In this section, we compare the performance corresponding to the two models of channels defined by (42) and (43). We initialize the POPS algorithm with the most localized Gaussian vector, $\left[\boldsymbol{\varphi}^{(0)}\right]_k = 2^{1/4}e^{-2\pi t_k^2}$, where $t_k = kT_s$ with $k \in [\![-(P-1)/2, (P-1)/2]\!]$, $P = ND_{\text{OQAM}} = DQ$, and a sampling period $T_s = 1/QF$. We remind that $N = Q/2$ is the number of subcarriers, and $D_{\text{OQAM}} = 2D$ is the number of periods in the support duration, (D is the normalized support duration), for FBMC/OQAM.

Figure 1 represents the evolution of the optimized SINR as a function of D, for uniform multipath power profile of the channel, where SNR $=$ 40 dB and $T = NT_s$, with $N = 256$. We note that the SINR stabilizes, for all B_dT_m values, at $D_{\text{OQAM}} = 4$ (i.e. $D = 8$), which corresponds to supports durations of $\boldsymbol{\varphi}$ and $\boldsymbol{\psi}$ equal to $8T$. Therefore, we stop the optimization at $D = 4$, for FBMC/OQAM. We note that the curves are so flat that a significant reduction in the value of D causes a slight degradation. That makes FBMC/OQAM more interesting since we can reduce the processing time, complexity, and latency without degrading the performance. We notice also that by decreasing the time-frequency dispersions, the SINR increases and becomes close to the SNR value when B_dT_m is below 10^{-4}, since the interference tends to 0. On the other hand, we remark that the obtained SINR remains high enough, even for large time and frequency dispersions ($B_dT_m = 10^{-2}$), which makes it possible to work comfortably with 2-ASK or 4-ASK modulations, without needing equalization or CP insertion, as proposed in [26].

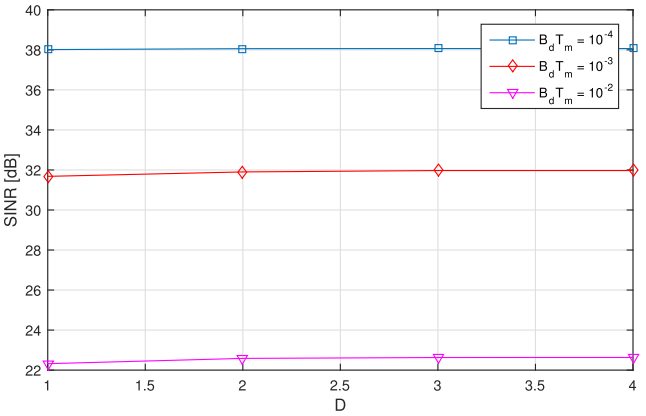

FIGURE 1. SINR as a function of D, for $Q = 512$ and SNR $= 40$ dB.

In Figure 2, we compare the optimized SINR for uniform and exponential channels (see (42) and (43) expressions). For each case, we increase D until stabilization of the SINR. For the exponential channel, the SINR stabilizes also at $D = 4$. Numerical results in this figure show that for low time-frequency dispersions ($B_dT_m = 10^{-4}$), the two systems become equivalent in terms of SINR. However, for high time-frequency dispersions ($B_dT_m = 10^{-2}$), the SINR of exponential channel exceeds the SINR of uniform channel by 3.4 dB. In fact, the uniform channel is the most entropic channel.

In Figure 3, we present the optimal Tx waveforms, $\boldsymbol{\varphi}_{opt}$, maximizing the SINR, for D in $[\![1, 4]\!]$. We remark that the optimal Tx waveforms, resulting from Algorithm 1, decay linearly in time and frequency, in the logarithmic scale, by increasing D. This behavior has also been observed in the continuous-time context, but there was some doubt whether this behavior was intrinsic to the optimized waveforms, or was really inherited from the way in which the signal space was explored. Indeed, Hermite functions are known to decrease exponentially in time and frequency. In addition to that, we note that the optimal Tx waveforms are localized in time even for $D = 2$, which is important in the case of practical hardware realizations. Therefore, with a reduced support duration, we obtain almost the same performance in terms of SINR.

B. FBMC/OQAM SYSTEMS VS. FBMC/QAM SYSTEMS

To compare FBMC/OQAM to FBMC/QAM systems, we represent in Figure 4 the evolution of the optimal SINR as a function of B_dT_m, for SNR $=$ 30 dB and different value of FT for FBMC/QAM systems. This Figure is obtained by selecting the optimal value of the SINR reached for each value of B_dT_m. For $B_dT_m = 10^{-2}$ and the critical density, FBMC/OQAM outperforms FBMC/QAM by 4 dB. On the other hand, this gain fades when reducing the lattice density

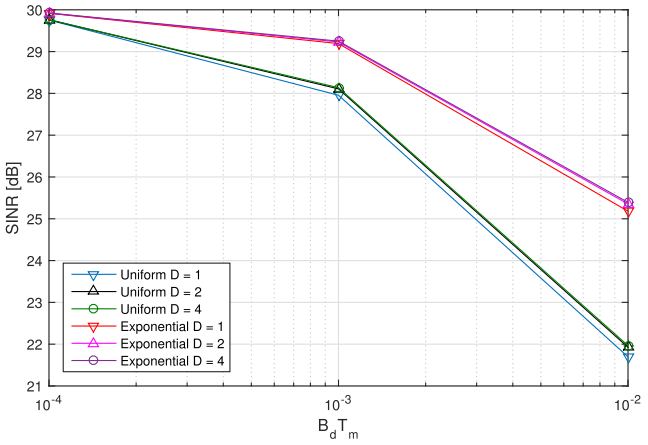

FIGURE 2. SINR as a function of D, for uniform vs. exponential channel, and SNR = 30 dB.

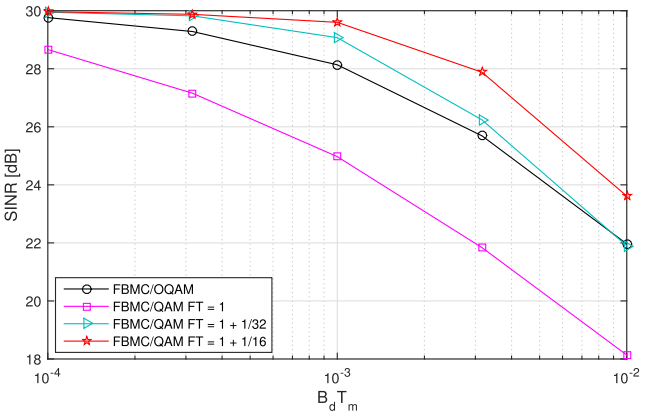

FIGURE 4. Optimal SINR of FBMC/OQAM vs. FBMC/QAM, as a function of $B_d T_m$, for SNR = 30 dB.

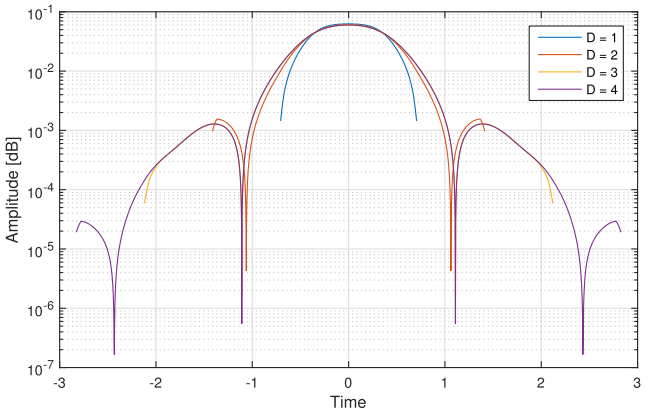

FIGURE 3. Amplitude of φ, for $B_d T_m = 10^{-2}$, $Q = 512$, SNR = 30 dB and $D = 1, \ldots, 4$.

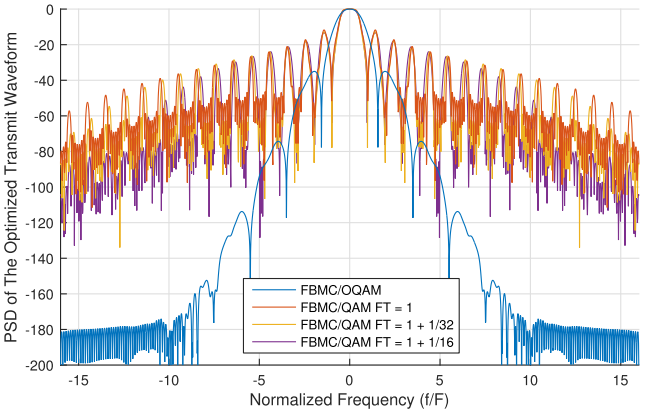

FIGURE 5. PSD of one subcarrier for SNR = 30 dB, $B_d T_m = 10^{-2}$, $Q = 512$, and $D = 8$.

to $\Delta = 1/(1 + 1/32) \simeq 0.97$, contrary to the continuous-time case, the SINR of FBMC/QAM is equal to that of FBMC/OQAM, for $B_d T_m = 10^{-2}$. We note that, although the performance has improved for FBMC/QAM compared to the critical case, we obtain better performance in the discrete-time, when reducing the lattice density by 3%, than in the continuous-time version. Indeed, the way to sweep the space in the discrete-time is more efficient than in the continuous-time, and the processing is more faster in the discrete-time, which allows to reach better results. Finally, for $\Delta = 1/(1 + 1/16) \simeq 0.94$, FBMC/QAM outperforms FBMC/OQAM by 1.65 dB, for $B_d T_m = 10^{-2}$. Therefore, we note that the reduction of the spectral efficiency by almost 4% allows to obtain the same performance. This reduction can be justified in practice in terms of complexity, since FBMC/QAM is easier to use in multiple-input and multiple-output (MIMO) systems.

Numerical results in Figure 5 show that the optimal Tx waveform of FBMC/OQAM is more localized in frequency. Thus, it reduces the OOB emissions with respect to Tx waveforms of FBMC/QAM. We note that by increasing the lattice density, Δ, for FBMC/QAM, we lose frequency localization for high frequencies. We note that we took the case of single user with comparable power density of the subcarriers at Tx. However, when we want to use our optimized waveforms in the case of multiple access, if we have an imbalance in the power density for users that can in practice reach 20 dB, we will have problems with the FBMC/QAM because the waveforms are not well localized in frequency. In contrast, for FBMC/OQAM, the frequency localization is sufficiently excellent to circumvent the problem of interference between users.

C. FBMC/OQAM SYSTEMS: CONTINUOUS-TIME VS. DISCRETE-TIME

In Figure 6, we compare the optimal SINR obtained for discrete-time, for $D = 4$, with continuous-time, using $K = 17$ Hermite functions, as a function of $B_d T_m$, for different SNR values and the uniform channel. We remark that the obtained results are identical for the two systems. Therefore, these two systems are equivalent. Moreover, we note that when the SINR tends to 0, we have an asymptote equal to the SNR, which is clear for SNR = 20 dB and SNR = 30 dB. This is not the case for SNR = 40 dB because we have not reduced enough the values of $B_d T_m$.

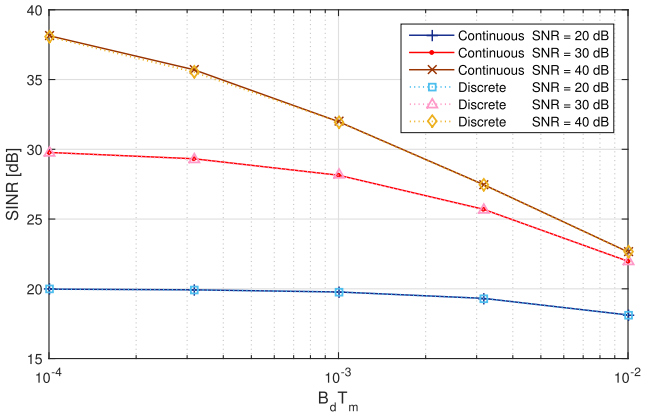

FIGURE 6. Optimal SINR of FBMC/OQAM for continuous-time vs. discrete-time as a function of $B_d T_m$, for SNR = 20, 30 and 40 dB.

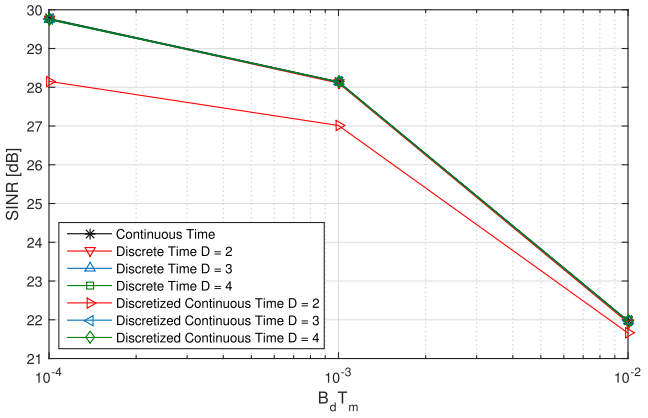

FIGURE 7. Optimal SINR of FBMC/OQAM systems for continuous-time vs. discrete-time vs. discretized continuous time versions, as a function of $B_d T_m$, for SNR = 30 dB.

To obtain Figure 7, we sample the optimal Tx/Rx waveforms reached in the continuous-time, for $K = 17$ Hermite functions, with a sampling period $T_s = 1/QF$, and using the same time axis t defined in Section VI-A. Then, we calculate the SINR of these waveforms, after truncation for $D = 2, 3$ and 4, using the discrete-time SINR expressions. We refer to the obtained system by ''discretized continuous time'' in the legend. Using the ''discretized continuous time'' waveforms, we reach the same optimal SINR values for $D = 3$ and 4 compared to the continuous- and directly optimized discrete-time systems. However, for $D = 2$, we lose 1.6 dB, in terms of SINR, for $B_d T_m = 10^{-4}$.

VII. CONCLUSION

In this paper, we studied the performance of the FBMC/OQAM and FBMC/QAM systems, in the discrete-time context, using an arbitrary WSSUS discrete-time propagation channel. This work brings many benefits and insights with respect to a previous work [7] on waveforms optimization for continuous-time FBMC/OQAM and FBMC/QAM systems.

First of all, we stood out from the previous work on the continuous-time context by searching for the best Tx/Rx waveforms through a perfect exploration of the finite dimension signal space, stemming from their finite support discrete-time nature. In contrast, we recall that space exploration was far from being perfect for FBMC/QAM operating at critical or near-critical lattice densities, for which optimal waveforms are known to be poorly localized. Indeed, the orthonormal base of very well time-frequency localized Hermite functions was at the origin of a bad exploration of the signal space from which the poorly localized optimal waveforms should be identified.

Secondly, the discrete-time finite-support optimal waveforms, obtained in this paper, have the merit of being ready-to-use, and do not need any further processing for their implementation in practice. We recall that, in the continuous-time context, the obtained waveforms are of infinite time support. Therefore, they need to be sampled and truncated in time prior to any practical use. As it is known, truncation in time can be very severe in the case of low latency systems. For such severe truncations, we noticed a significant decrease in optimized SINR for FBMC/QAM, due to poor waveform localization in this case. Although it is not covered in this paper, truncation in time is expected to bring an increase in OOB emissions, which can be detrimental in practice, especially in the presence of multi-users access. Fortunately, for FBMC/OQAM, the system was enough robust, that we observed a preservation of SINR performance, even for severe truncations.

The present work on discrete-time framework allowed an identical exploration of the signal space for FBMC/OQAM and FBMC/QAM. Therefore, it ensured a fair comparison of these systems. Indeed, we used the same supports durations and the same number of samples to compare the two systems. Thus, we were able to accurately reveal the true gains brought by FBMC/OQAM with respect to FBMC/QAM. For example, we noticed that FBMC/OQAM systems present a gain of 4 dB in SINR for low channel dispersions, and 1 dB for relatively high dispersions, when both operate at critical time-frequency lattice densities. We point out that this was not possible for FBMC/QAM, in the continuous-time context for FBMC/QAM, where the optimized SINR does not stabilize, even if a gigantic number of Hermite functions is used for signal space exploration.

We have also noticed in this work that, in order to boost FBMC/QAM to achieve the same performance of FBMC/OQAM, a sacrifice of spectral efficiency of less than 4% was sufficient. This is, in fact, in perfect agreement with the previous work in the continuous-time framework. Again, this reduction, which is deemed to be insignificant, has the merit of offering a significant reduction in reception complexity, when FBMC/QAM is used instead of FBMC/OQAM, especially in the MIMO context.

In addition to all previously mentioned advantages, this paper allowed a cross-validation of the present work on discrete-time with the previous work on continuous-time. Indeed, comparable results were obtained for FBMC/OQAM due to an almost perfect, and therefore similar exploration of the signal space in the two contexts. In addition to that,

this work revealed that, contrary to the continuous-time framework, the SINR expressions for the optimization of the Rx waveform, given the Tx waveform, and the Tx waveform, given the Rx waveform, are not symbolically identical. Finally, some of the obtained results brought to light an exponential decrease in time for optimized FBMC/OQAM waveforms in the discrete case, where the signal space was freely and fully explored, without any constraints. We recall that this exponential decrease was also observed in the continuous-time context. We underline that, at the time when the work on the continuous-time context was carried out, it was not possible to argue whether the observed exponential decay was really an intrinsic property of the optimized waveforms or an inheritance of the exponential decay of the Hermite functions, used for signal space exploration.

APPENDIX A
DERIVATION OF THE USEFUL AND INTERFERENCE POWERS IN FBMC/OQAM SYSTEMS

In this Appendix, we provide the derivation of the useful and interference powers in FBMC/OQAM systems, i.e. P_U and P_I. We set $X = \sum_{l=0}^{L-1} c_l e^{j\pi\nu_l T_s p_l}$; $Y_{mn} = \langle \boldsymbol{\psi}_{00}, \tilde{\boldsymbol{\varphi}}_{mn} \rangle$; and $P_{mn} = \frac{E}{2\|\varphi\|^2}\mathbb{E}\left[\left(\Re\left\{e^{-j\chi_{00}}\langle \boldsymbol{\psi}_{00}, \tilde{\boldsymbol{\varphi}}_{mn}\rangle\right\}\right)^2\right]$.

Since the compensation factor is given by $e^{j\chi_{00}} = X/|X|$ (see (8)), we can write

$$P_{mn} = \frac{E}{2\|\varphi\|^2}\mathbb{E}\left[\left(\Re\left\{\frac{X^*}{|X|}Y_{mn}\right\}\right)^2\right]. \tag{A.1}$$

We find the expression (A.9) in [7], given by

$$\mathbb{E}\left[\left(\Re\left\{\frac{X^*}{|X|}Y_{mn}\right\}\right)^2\right] = \frac{1}{2}\left(\frac{\Re\left\{\left(\mathbb{E}\left[X^*Y_{mn}\right]\right)^2\right\}}{\mathbb{E}\left[|X|^2\right]} + \mathbb{E}\left[|Y_{mn}|^2\right]\right). \tag{A.2}$$

As a result, P_{mn} will be given by

$$P_{mn} = \frac{E}{4\|\varphi\|^2}\left(\frac{\Re\left\{\left(\mathbb{E}\left[X^*Y_{mn}\right]\right)^2\right\}}{\mathbb{E}\left[|X|^2\right]} + \mathbb{E}\left[|Y_{mn}|^2\right]\right). \tag{A.3}$$

As $Y_{mn} = \sum_q \left[\boldsymbol{\psi}_{00}\right]_q^* \sum_{k=0}^{L-1} c_k \left[\boldsymbol{\varphi}_{mn}\right]_{q-p_k} e^{j2\pi\nu_k T_s\left(q+\frac{p_k}{2}\right)}$, the inter-correlation between X and Y_{mn} can be expressed as

$$\mathbb{E}\left[X^*Y_{mn}\right] = \sum_q \left[\boldsymbol{\psi}\right]_q^* \sum_{k=0}^{L-1} \pi_k \left[\boldsymbol{\varphi}_{mn}\right]_{q-p_k} e^{j2\pi\nu_k T_s q}. \tag{A.4}$$

We denote by $\boldsymbol{\xi}_\nu$ the complex vector defined as $\left(\boldsymbol{\xi}_\nu\right)_q = \left(e^{j2\pi\nu T_s q}\right)_q$. Using the time shift operator $\boldsymbol{\sigma}_p(\cdot)$, we can write

$$\mathbb{E}\left[X^*Y_{mn}\right] = \boldsymbol{\psi}^H\left(\sum_{k=0}^{L-1}\pi_k \boldsymbol{\xi}_{\nu_k} \odot \boldsymbol{\sigma}_{p_k}\left(\boldsymbol{\varphi}_{mn}\right)\right). \tag{A.5}$$

Hence, we obtain

$$\Re\left\{\left(\mathbb{E}\left[X^*Y_{mn}\right]\right)^2\right\} = \Re\left\{\boldsymbol{\psi}^H\left[\begin{array}{l}\left(\sum_{k=0}^{L-1}\pi_k \boldsymbol{\xi}_{\nu_k} \odot \boldsymbol{\sigma}_{p_k}\left(\boldsymbol{\varphi}_{mn}\right)\right) \\ \times\left(\sum_{l=0}^{L-1}\pi_l \boldsymbol{\xi}_{\nu_l} \odot \boldsymbol{\sigma}_{p_l}\left(\boldsymbol{\varphi}_{mn}\right)\right)^T\end{array}\right]\boldsymbol{\psi}^*\right\}. \tag{A.6}$$

Since the variance of X is

$$\mathbb{E}\left[|X|^2\right] = \sum_{k,l=0}^{L-1}\mathbb{E}\left[c_k^* c_l\right]e^{j\pi T_s(\nu_l p_l - \nu_k p_k)} = \sum_{l=0}^{L-1}\pi_l, \tag{A.7}$$

we can write

$$\frac{\Re\left\{\left(\mathbb{E}\left[X^*Y_{mn}\right]\right)^2\right\}}{\mathbb{E}\left[|X|^2\right]} = \frac{1}{\sum_{l=0}^{L-1}\pi_l}\Re\left\{\boldsymbol{\psi}^H\left[\begin{array}{l}\left(\sum_{k=0}^{L-1}\pi_k \boldsymbol{\xi}_{\nu_k} \odot \boldsymbol{\sigma}_{p_k}\left(\boldsymbol{\varphi}_{mn}\right)\right) \\ \times\left(\sum_{l=0}^{L-1}\pi_l \boldsymbol{\xi}_{\nu_l} \odot \boldsymbol{\sigma}_{p_l}\left(\boldsymbol{\varphi}_{mn}\right)\right)^T\end{array}\right]\boldsymbol{\psi}^*\right\}. \tag{A.8}$$

As $Y_{mn} = \boldsymbol{\psi}_{00}^H\tilde{\boldsymbol{\varphi}}_{mn} = \boldsymbol{\psi}^H\tilde{\boldsymbol{\varphi}}_{mn}$, the variance of Y_{mn} is

$$\mathbb{E}\left[|Y_{mn}|^2\right] = \boldsymbol{\psi}^H\mathbb{E}\left[\tilde{\boldsymbol{\varphi}}_{mn}\tilde{\boldsymbol{\varphi}}_{mn}^H\right]\boldsymbol{\psi}, \tag{A.9}$$

where

$$\mathbb{E}[[\tilde{\boldsymbol{\varphi}}_{mn}]_p[\tilde{\boldsymbol{\varphi}}_{mn}^H]_q] = \sum_{k=0}^{L-1}\pi_k\left[\boldsymbol{\varphi}_{mn}\right]_{p-p_k}\left[\boldsymbol{\varphi}_{mn}\right]_{q-p_k}^* e^{j2\pi\nu_k T_s(p-q)}. \tag{A.10}$$

By noting by $\boldsymbol{\Phi}_\nu$ the Hermitian matrix defined as $(\boldsymbol{\Phi}_\nu)_{pq} = \left(e^{j2\pi\nu T_s(p-q)}\right)_{pq}$, we can write

$$\mathbb{E}\left[\tilde{\boldsymbol{\varphi}}_{mn}\tilde{\boldsymbol{\varphi}}_{mn}^H\right] = \sum_{k=0}^{L-1}\pi_k\boldsymbol{\Phi}_{\nu_k} \odot \left(\boldsymbol{\sigma}_{p_k}\left(\boldsymbol{\varphi}_{mn}\right)\boldsymbol{\sigma}_{p_k}\left(\boldsymbol{\varphi}_{mn}\right)^H\right). \tag{A.11}$$

Therefore, the variance of Y_{mn} is given by

$$\mathbb{E}\left[|Y_{mn}|^2\right] = \boldsymbol{\psi}^H\left[\sum_{k=0}^{L-1}\pi_k\boldsymbol{\Phi}_{\nu_k} \odot \left(\boldsymbol{\sigma}_{p_k}\left(\boldsymbol{\varphi}_{mn}\right)\boldsymbol{\sigma}_{p_k}\left(\boldsymbol{\varphi}_{mn}\right)^H\right)\right]\boldsymbol{\psi}. \tag{A.12}$$

Finally, we inject (A.8) and (A.12) in (A.3). Thus, the final expression of P_{mn} is given by

$$P_{mn} = \frac{E}{4\|\varphi\|^2}\left(\begin{array}{l}\frac{1}{\sum_{l=0}^{L-1}\pi_l}\Re\left\{\boldsymbol{\psi}^H\left[\begin{array}{l}\left(\sum_{k=0}^{L-1}\pi_k \boldsymbol{\xi}_{\nu_k} \odot \boldsymbol{\sigma}_{p_k}\left(\boldsymbol{\varphi}_{mn}\right)\right) \\ \times\left(\sum_{l=0}^{L-1}\pi_l \boldsymbol{\xi}_{\nu_l} \odot \boldsymbol{\sigma}_{p_l}\left(\boldsymbol{\varphi}_{mn}\right)\right)^T\end{array}\right]\boldsymbol{\psi}^*\right\} \\ +\boldsymbol{\psi}^H\left[\sum_{k=0}^{L-1}\pi_k\boldsymbol{\Phi}_{\nu_k} \odot \left(\boldsymbol{\sigma}_{p_k}\left(\boldsymbol{\varphi}_{mn}\right)\boldsymbol{\sigma}_{p_k}\left(\boldsymbol{\varphi}_{mn}\right)^H\right)\right]\boldsymbol{\psi}\end{array}\right). \tag{A.13}$$

REFERENCES

[1] Y. Wu, S. Singh, T. Taleb, A. Roy, H. S. Dhillon, M. R. Kanagarathinam, and A. De, "6G mobile wireless networks," in *Computer Communications and Networks*. Cham, Switzerland: Springer, 2021, pp. 1–472.
[2] A. F. Demir, M. Elkourdi, M. Ibrahim, and H. Arslan, "Waveform design for 5G and beyond," in *5G Networks: Fundamental Requirements Enabling Technologies and Operations Management*. Hoboken, NJ, USA: Wiley, Sep. 2018, pp. 51–76.
[3] B. Saltzberg, "Performance of an efficient parallel data transmission system," *IEEE Trans. Commun. Technol.*, vol. CT-15, no. 6, pp. 805–811, Dec. 1967.
[4] W. Saad, M. Bennis, and M. Chen, "A vision of 6G wireless systems: Applications, trends, technologies, and open research problems," *IEEE Netw.*, vol. 34, no. 3, pp. 134–142, Feb. 2019.
[5] J. J. Benedetto, C. Heil, and D. F. Walnut, "Differentiation and the Balian-Low theorem," *J. Fourier Anal. Appl.*, vol. 1, no. 4, pp. 355–402, 1994.
[6] X. Xu, Y. Pan, P. P. M. Y. Lwin, and X. Liang, "3D holographic display and its data transmission requirement," in *Proc. Int. Conf. Inf. Photon. Opt. Commun.*, Oct. 2011, pp. 1–4.
[7] W. Khrouf, M. Siala, and F. Abdelkefi, "How much FBMC/OQAM is better than FBMC/QAM? A tentative response using the POPS paradigm," *Wireless Commun. Mobile Comput.*, vol. 2018, pp. 1–14, Apr. 2018.
[8] A. Hilario-Tacuri, "Computational tool for the evaluation of waveform candidates of beyond 5G and 6G systems," in *Proc. IEEE 28th Int. Conf. Electron., Electr. Eng. Comput. (INTERCON)*, Aug. 2021, pp. 1–4.
[9] *FANTASTIC-5G*. Accessed: Sep. 1, 2022. [Online]. Available: http://fantastic5g.com/
[10] *METIS*. Accessed: Sep. 1, 2022. [Online]. Available: https://metis2020.com/
[11] *5GNOW*. Accessed: Sep. 1, 2022. [Online]. Available: http://5gnow.eu/
[12] B. Farhang-Boroujeny, "OFDM versus filter bank multicarrier," *IEEE Signal Process. Mag.*, vol. 28, no. 3, pp. 92–112, May 2011.
[13] B. Le Floch, M. Alard, and C. Berrou, "Coded orthogonal frequency division multiplex," *Proc. IEEE*, vol. 83, no. 6, p. 982–996, Jun. 1995.
[14] D. Chen, Y. Tian, D. M. Qu, and T. Jiang, "OQAM-OFDM for wireless communications in future Internet of Things: A survey on key technologies and challenges," *IEEE Internet Things J.*, vol. 5, no. 5, pp. 3788–3809, Oct. 2018.
[15] Z. He, L. Zhou, Y. Chen, and X. Ling, "Filter optimization of out-of-band emission and BER analysis for FBMC-OQAM system in 5G," in *Proc. IEEE 9th Int. Conf. Commun. Softw. Netw. (ICCSN)*, May 2017, pp. 56–60.
[16] S. S. K. C. Bulusu, H. Shaiek, D. Roviras, and R. Zayani, "Reduction of PAPR for FBMC-OQAM systems using dispersive SLM technique," in *Proc. 11th Int. Symp. Wireless Commun. Syst. (ISWCS)*, Oct. 2014.
[17] M. Bellanger, "FBMC physical layer: A primer," *PHYDYAS Project*, vol. 25, no. 4, pp. 7–10, Jun. 2010.
[18] S. Mirabbasi and K. Martin, "Overlapped complex-modulated transmultiplexer filters with simplified design and superior stopbands," *IEEE Trans. Circuits Syst. II, Analog Digit. Signal Process.*, vol. 50, no. 8, pp. 456–469, Aug. 2003.
[19] R. Ravindran and A. Viswakumar, "Performance evaluation of 5G waveforms: UFMC and FBMC-OQAM with cyclic prefix-OFDM system," in *Proc. 9th Int. Conf. Adv. Comput. Commun. (ICACC)*, Nov. 2019.
[20] Z. Hraiech, F. Abdelkefi, M. Siala, and R. Zayani, "Optimization of the PHYDYAS waveforms using the POPS algorithm: POPS-PHYDYAS," in *Proc. 15th Int. Multi-Conf. Syst., Signals Devices (SSD)*, Mar. 2018.
[21] J. Zhao, S. Ni, and Y. Gong, "Peak-to-average power ratio reduction of FBMC/OQAM signal using a joint optimization scheme," *IEEE Access*, vol. 5, pp. 15810–15819, 2017.
[22] D. Qu, F. Wang, Y. Wang, T. Jiang, and B. Farhang-Boroujeny, "Improving spectral efficiency of FBMC-OQAM through virtual symbols," *IEEE Trans. Wireless Commun.*, vol. 16, no. 7, pp. 4204–4215, Jul. 2017.
[23] M. Siala, F. Abdelkefi, and Z. Hraiech, "Novel algorithms for optimal waveforms design in multicarrier systems," in *Proc. IEEE Wireless Commun. Netw. Conf. (WCNC)*, Apr. 2014.
[24] R. Zakaria, "Conception d'Emetteur et récepteur pour l'Elimination des interférences intrinsèques dans les systèmes multiporteuses à base de bancs de filtres et à antennes multiples," Ph.D. dissertation, Ecole Doctorale Technologique et Professionnelle, Cedric/Laetitia, France, Nov. 2012.
[25] P. A. Bello, "Characterization of randomly time-variant linear channels," *IEEE Trans. Commun. Syst.*, vol. CS-11, no. 4, pp. 360–393, Dec. 1963.
[26] D. Chen, X.-G. Xia, T. Jiang, and X. Gao, "Properties and power spectral densities of CP based OQAM-OFDM systems," *IEEE Trans. Signal Process.*, vol. 63, no. 14, pp. 3561–3575, Jul. 2015.

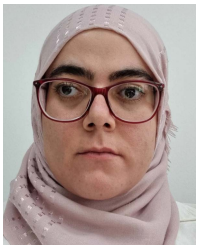

WAFA KHROUF (Member, IEEE) received the Engineering degree in telecommunication engineering and the Ph.D. degree (Hons.) from the Higher School of Communications of Tunis (SUP'COM), Tunisia, in 2014 and 2019, respectively. Her research interests include the areas of digital and wireless communications with special emphasis on waveform design for FBMC systems. She holds one article in *Wireless Communications and Mobile Computing* journal and four IEEE conferences.

MOHAMED SIALA (Senior Member, IEEE) received the General Engineering degree from École Polytechnique, Palaiseau, France, in 1988, and the Specialization Engineering degree in telecommunications and the Ph.D. degree in digital communications from Télécom ParisTech, Paris, France, in 1990 and 1995, respectively. From 1990 to 1992, he was at Alcatel Radio-Telephones, Colombes, France, working on the implementation of the GSM physical layer. In 1995, he joined Wavecom, Issy-les-Moulineaux, France, where he worked on advanced multicarrier communications and channel estimation for low-orbit mobile satellite communications. From 1997 to 2001, he worked at Orange Laboratories, Issy-les-Moulineaux, on the assessment of the performance of the physical layer of 3G systems and participated actively in their standardization. In 2001, he joined SUP'COM, Tunis, Tunisia, where he is currently a Full Professor. His research interests include the areas of digital and wireless communications with special emphasis on waveform design for advanced multicarrier systems and ARQ, channel estimation, synchronization, adaptive modulation and coding, MIMO systems, massive MIMO, space–time coding, relaying, cooperative networks, and cognitive radio. He holds respectively 40 and 221 papers in prestigious journals and conferences and six patents.

FATMA ABDELKEFI (Senior Member, IEEE) received the Engineering degree in electrical engineering from the Ecole Nationale d'Ingénieurs de Tunis, Tunis, Tunisia, in 1998, the M.S. degree in digital communications systems and the Ph.D. degree (Hons.) from the Ecole Nationale Supérieure de Télécommunications, Paris, France, in 1999 and 2002, respectively. She was a Research Assistant with the Signals and Systems Laboratory of SUPELEC, Gif-sur-Yvette, France. In November 2002, she joined the Signal Processing Group, Ecole Nationale Supérieure de l'Electronique et de ses Applications, Paris, as a Research Associate. She spent two years with the Communication Technology Laboratory, Swiss Federal Institute of Technology, Zurich, Switzerland, and she was a Scientific Collaborator with the Ecole Polytechnique Fédérale de Lausanne, Lausanne, Switzerland. Since 2008, she has been with the Higher School of Communications of Tunis, Tunisia, where she is currently an Associate Professor. She is also an Associate Researcher with the Signal and Communications Department, Telecom-Bretagne, France. Her research interests include advanced signal processing techniques, compressed sensing theory, digital communications, information theory, detection and estimation, and multicarrier systems.